Angularly resolved Auger rates of LiF and HF

K. Zähringer, H.-D. Meyer, and L. S. Cederbaum
Theoretische Chemie, Physikalisch Chemisches Institut, Universität Heidelberg, Im Neuenheimer Feld 253, W-6900 Heidelberg, Federal Republic of Germany
(Received 27 March 1992)

Angularly resolved Auger rates are investigated. The angular distributions of Auger electrons display a strong dependence on the final dicationic state which is created by the Auger process. The angular distributions show interference structures which can be related to the geometry of the molecule. Although there are presently no experimental data on angularly resolved Auger rates, we suppose that the angular distributions are measurable, e.g., by coincidence techniques.

PACS number(s): 33.80.Eh, 32.80.Hd, 34.80.Kw

I. INTRODUCTION

The investigation of Auger spectra of molecules is an active field both experimentally [1,2] and theoretically [2,3]. From a theoretical point of view the computation of Auger spectra can be split into three parts, namely, (i) the computation of fixed-nuclei Auger energies, (ii) the computation of fixed-nuclei Auger intensities, and (iii) the inclusion of the nuclei motion. The vertical Auger energies can be computed by standard [4] and less standard [5] quantum-chemistry methods. The computation of the Auger intensities is less straightforward because it requires the knowledge of the continuum wave of the Auger electron. The nuclear motion is responsible for the width of the molecular Auger lines (the natural width is almost negligible). It also may introduce important shifts of the positions of the lines [6]. The nuclear dynamics associated with the Auger process has been ignored in almost all investigations. A systematic and feasible approach to account for the nuclear dynamics was introduced only recently [6]. In the present investigation we will ignore the nuclear motion, concentrate on the Auger intensities, and discuss the Auger energies only in passing.

All the previous investigations have dealt with angularly integrated molecular Auger spectra. There are—to our knowledge—no investigations on angularly resolved Auger spectra of (free) molecules, neither theoretically nor experimentally. A first step towards angularly resolved Auger spectra is the experimental determination of the asymmetry parameters β [2,7]. Here a core-excited state is produced by absorption of a polarized photon. Since the absorption probability depends on the molecular orientation with respect to the polarization vector there arises some correlation between the polarization vector and the asymptotic momentum of the Auger electron [2,7]. However, the full angular distribution of Auger electrons should be also measurable, e.g., by detecting in coincidence the momenta of the Auger electron and of the atomic ion that is formed when the (diatomic) molecule dissociates immediately after the Auger electron is emitted. Another possible way to fix the molecular orientation is to adsorb the molecule on a crystal surface. Depending on the particular molecule and crystal one may find the molecules to be oriented in a well-defined direction [8]. The theoretical study of angularly resolved Auger spectra of adsorbed molecules is, however, more difficult because the influence of the surface on the Auger electrons cannot be neglected [9]. It is clear that the angularly resolved Auger spectra provide more information on the electronic structure than the integrated rates. In particular, the assignment of the Auger lines to the final dicationic states is easier when angularly resolved spectra are available.

In this article we report calculated angularly resolved Auger spectra of LiF and HF. Our theoretical and numerical approach is outlined in a recent publication [10] and will be briefly reviewed in Sec. II. The shape of the angular distribution can be thought of as being generated by two processes. The first one is the Auger transition itself. A nonspherical distribution arises because the molecular orbitals are not spherically symmetric. In a second step the ejected electron is deflected by the presence of the electron-molecule potential. These two effects are discussed in comparison in Sec. III. In Sec. IV we discuss the angular distribution of the Auger electrons of LiF when the final dicationic state contains a 2σ hole, i.e., when an electron is removed from the Li-core orbital. Since the two missing electrons of the final state come from orbitals which are centered at different nuclei, one observes new structures in the angular distribution. In Sec. V we briefly discuss the angularly integrated Auger spectrum of LiF for the sake of completeness and in Sec. VI we finally conclude our findings.

II. THE COMPUTATION OF AUGER INTENSITIES

Our theoretical and numerical approach to the computation of Auger intensities is built on the following approximations (see Ref. [10] for details).

(i) The Auger effect is considered as a two-step process (ionization and decay).

(ii) A nonrelativistic first-order treatment of the decay (Wentzel's ansatz) is adopted.

(iii) The ejected Auger electron is not allowed to correlate with the other electrons of the residual dication and a single-channel approximation is assumed to be sufficient.

Apart from these approximations we evaluate the initial core-ionized state and the final dicationic states by the self-consistent-field (SCF) method. The continuum wave function of the Auger electron was computed by adopting the static-exchange potential [11] as interaction. The exchange potential, however, was replaced by a local model potential [11,12]. The basis set used here for LiF is discussed in Sec. V, the one for HF is discussed in Ref. [10].

We now give our final working equations (see Ref. [10] for a comprehensive derivation). The angularly resolved Auger rate is given by

$$\frac{d\sigma}{d\Omega}=2\pi\left|\sum_{l,m}A_{l,m}Y_{l,m}(\Omega)\right|^2 , \tag{2.1}$$

where in the case of a linear molecule there is only one m term in the above sum which contributes; $m=0$ for final Σ states, $m=1$ for final Π states, etc. For linear molecules the angle is measured with respect to the molecular axis. The symbol $Y_{l,m}$ denotes the spherical-harmonic function and $A_{l,m}$ is the Auger amplitude which—depending on the final state—is given by one of the following three cases.

Case (a). Singlet, both electrons removed from the same spatial orbital n,

$$A_{l,m}=\sum_{j,k}^{\text{occ}}V(\varepsilon_\perp,l,m)_{j,k}Q_{j,k}^{n,n} . \tag{2.2a}$$

Case (b). Singlet, electrons removed from different spatial orbitals n and n',

$$A_{l,m}=(\tfrac{1}{2})^{1/2}\sum_{j,k}^{\text{occ}}[V(\varepsilon_\perp,l,m)_{j,k}+V(\varepsilon_\perp,l,m)_{k,j}]Q_{j,k}^{n,n'} . \tag{2.2b}$$

Case (c). Triplet

$$A_{l,m}=(\tfrac{3}{2})^{1/2}\sum_{j,k}^{\text{occ}}[V(\varepsilon_\perp,l,m)_{j,k}-V(\varepsilon_\perp,l,m)_{k,j}]Q_{j,k}^{n,n'} . \tag{2.2c}$$

The symbol V denotes a Coulomb matrix element [atomic units (a.u.) are used throughout],

$$V(\varepsilon,l,m)_{j,k}=\int d\mathbf{r}\,d\mathbf{r}'[\varphi_c(\mathbf{r})]^*[\psi_{\varepsilon,l,m}^-(\mathbf{r}')]^*\times|\mathbf{r}-\mathbf{r}'|^{-1}\varphi_j(\mathbf{r})\varphi_k(\mathbf{r}') \tag{2.3}$$

and

$$V(\varepsilon_\perp,l,m)_{j,k}=V(\varepsilon,l,m)_{j,k}-\sum_{i}^{\text{occ}}V_{c,i,j,k}\langle\psi_{\varepsilon,l,m}^-|\varphi_i\rangle , \tag{2.4}$$

where

$$V_{i,j,k,l}=\int d\mathbf{r}\,d\mathbf{r}'[\varphi_i(\mathbf{r})]^*[\varphi_j(\mathbf{r}')]^*|\mathbf{r}-\mathbf{r}'|^{-1}\varphi_k(\mathbf{r})\varphi_l(\mathbf{r}') \tag{2.5}$$

In the above equations the φ's denote the orbitals of the initial (core-ionized) state and φ_c is the core orbital from which initially an electron was removed. [The index c does not appear at the symbol $V(\varepsilon,l,m)$ since it is fixed.] The summations in Eqs. (2.2)–(2.5) run over all orbitals which are occupied in the initial core-ionized state. The symbol $\psi_{\varepsilon,l,m}^-$ denotes the wave function of an Auger electron of energy ε and asymptotic angular momentum (l,m). The minus sign indicates the incoming boundary condition of this state. $\psi_{\varepsilon,l,m}^-$ is generated by integration of the closed-coupled equations [10,13] while adopting the static-exchange potential (with a local model exchange) as interaction. Equation (2.4) merely orthogonalizes the scattered wave $\psi_{\varepsilon,l,m}^-$ to the occupied orbitals of the *initial* state.

The matrix Q accounts for the nonorthogonality between the sets of orbitals of the initial and final state, respectively. Q is given by

$$Q_{j,k}^{n,n'}=(\mathbf{S}^{-1})_{j,n}(\mathbf{S}^{-1})_{k,n'}[\det(\mathbf{S})]^2 , \tag{2.6}$$

where $S_{i,j}=\langle\chi_i|\varphi_j\rangle$ denotes the overlap matrix between the SCF orbitals $\{\varphi_j\}$ of the initial state and the ones $\{\chi_j\}$ of the particular final state under discussion, i.e., that final dicationic state that has a missing electron in the nth and n'th orbital. Note that by $\mathbf{S}$ we denote the overlap matrix truncated to the set of occupied orbitals, i.e., $\mathbf{S}$ is a $N/2\times N/2$ matrix where N denotes the number of electrons of the neutral closed shell target (see the appendix of Ref. [10] for details).

We used Eqs. (2.1)–(2.6) in the present calculations. For *interpretative* purposes it is, however, convenient to ignore the reorthogonalization of the continuum wave and to set the overlap matrix $\mathbf{S}$ equal to the unit matrix. With these simplifications Eq. (2.1) becomes

$$\frac{d\sigma}{d\Omega}\sim\left|\sum_{l,m}[V(\varepsilon,l,m)_{n,n'}\pm V(\varepsilon,l,m)_{n',n}]Y_{l,m}(\Omega)\right|^2 , \tag{2.7}$$

where the plus (minus) sign is to be taken in case of a singlet (triplet) state. If there is only a single angular-momentum term which contributes to the single-center expansion of the orbitals φ_c, φ_n, and $\varphi_{n'}$ (this is true for atomic targets) or if such a single term largely dominates then there will be only one or only few l terms that contribute to the sum (2.7). Separating angular from radial integration in Eq. (2.3) and recognizing that the single-center expansion (with origin at the F nuclei) of the flourine core orbital φ_c is dominated by the $(l=0,m=0)$ term, we obtain

$$V(\varepsilon,l,m)_{n,n'}=W_{n,n',l}\int d\Omega[Y_{l,m}(\Omega)]^*Y_{l_n,m_n}(\Omega)\times Y_{l_{n'},m_{n'}}(\Omega) , \tag{2.8}$$

where (l_n,m_n) and $(l_{n'},m_{n'})$ denote the angular momenta of the orbitals φ_n and $\varphi_{n'}$, respectively. $W_{n,n',l}$ denotes some radial integral and is of no further interest. The above angular integral does not vanish only if the triangular rule

$$|l_n-l_{n'}|\le l\le|l_n+l_{n'}| \tag{2.9}$$

and the conditions

$$l+l_n+l_{n'}=\text{even} , \tag{2.10}$$

$$m=m_n+m_{n'} \tag{2.11}$$

are obeyed. The above selection rules ensure that there are only one or two terms that significantly contribute to the sum (2.7). If, for example, $l_n=0$, $m_n=0$, and $l_{n'}=1$, $m_{n'}=1$ holds, we deduce from Eqs. (2.7)–(2.11) that $d\sigma/d\Omega \sim |Y_{1,1}(\Omega)|^2$ is obeyed. We shall call an angular distribution that is given by the square of a spherical-harmonic function a "basic structure." We shall discuss basic structures in more detail in the following section.

III. ANGULAR DISTRIBUTIONS

The shape of the angular distributions of the Auger electrons can be thought of being generated by two processes. The first one is the Auger transition itself. A nonspherical symmetric distribution may arise because the molecular orbitals are not spherically symmetric in general. In a second step the ejected electron is deflected by the presence of the electron-molecule potential of the final dication. The first effect can be separated from the second one by assuming a vanishing electron-molecule interaction potential, i.e., by using plane waves for the scattered wave ψ^-. Although we know from our previous work [10] that the use of plane waves may yield unreliable Auger rates, we feel that the plane-wave approximation will show us what the *shape* of the angular distribution looks like if created by the first step alone.

Let us begin with discussing the angular distribution of the Auger electron of the LiF $^1\Sigma(3\sigma^{-2})$ dicationic state. The 3σ orbital has only little molecular character and is—similar to the 1σ core orbital—almost an atomic fluorine s-type orbital. (By the way, the 2σ orbital is the core orbital of the Li atom.) Because of the spherical symmetry of the 1σ and 3σ orbitals one expects from the first process alone a uniform distribution of Auger electrons, i.e., $d\sigma/d\Omega \sim |Y_{0,0}(\Omega)|^2 \equiv (4\pi)^{-1}$. As shown in Fig. 1(a), this is in fact what one gets when adopting the plane-wave approximation (dotted line). The solid line in Fig. 1(a) shows the angular distribution when accounting for the electron-molecule interaction potential. The intensity is enhanced in the forward direction—this is the direction from F to Li. More interesting are the oscillations on top. These are caused by the interference of two electron paths. The first path goes directly from the vicinity of the F nucleus to the detector. The second path goes first to the vicinity of the Li nucleus and is there deflected into the direction of the detector. With simple arguments known from the two-slits experiment one arrives at the following equations for the maxima and minima of the interference pattern ($n=0,1,\ldots$)

$$\cos\theta_{n,\max}=1-2n\pi/k_{\text{av}}R \tag{3.1}$$

and

$$\cos\theta_{n,\min}=1-(2n+1)\pi/k_{\text{av}}R . \tag{3.2}$$

Here R denotes the internuclear distance and k_{av} is some averaged wave number of the Auger electron. For the sake of simplicity k_{av} may be set equal to the asymptotic wave number $k=\sqrt{2\varepsilon}$. Improved values can be obtained by simply assuming a dicationic Coulomb potential on the fluorine atom and evaluating $k_{\text{av}}R$ by WKB

$$k_{\text{av}}R=\int_0^R \sqrt{2(\varepsilon+2/r)}dr . \tag{3.3}$$

More elaborate forms of the interference structure than in (3.1)–(3.3) can be derived, but are beyond the scope of this paper. Table I compares the locations of the minima and maxima determined with Eqs. (3.1)–(3.2) with those deduced from the full calculation. In order to find the correct positions of these latter extrema one has to subtract the nonconstant "background" on top of which the oscillations can be observed. This "background" distribution can be very conveniently generated by performing a scattering calculation in which the Li atom is removed as a localized center by simply averaging the scattering potential over the angles. (The origin of the coordinate system is at the F nucleus.) Figure 1(a) shows the result of such a calculation (dashed line) and the positions given in Table I are those of the extrema of the difference between the solid and the dashed curves. This difference is displayed in Fig. 2. The agreement between the positions of the simple model and of the full calculation is satisfying, showing that the explanation of the oscillations is correct.

Figure 1(b) shows similar angular distributions as Fig. 1(a) but for the $^1\Sigma(3\sigma^{-1},4\sigma^{-1})$ final state. The 4σ orbital correlates to the p_z orbital of F^-, hence its dominant angular momentum is $l=1$. By inspection of Eqs.

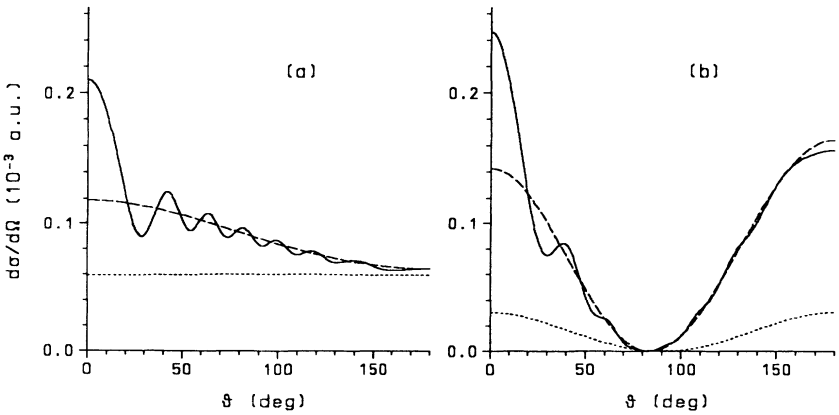

FIG. 1. Shown are the computed angularly resolved Auger spectra of the $^1\Sigma(3\sigma^{-2})$ state (a) and the $^1\Sigma(3\sigma^{-1},4\sigma^{-1})$ state (b) of the LiF molecule. For these final states we compare the result of the full calculation (solid line) with the nonconstant background (dashed line) on top of which the oscillations of the interference structure can be observed. The angular distributions of the plane-wave calculations are illustrated by the dotted curves (see text). The angle θ is the angle between the final momentum of the Auger electron and the internuclear axis. $\theta=0°$ denotes the direction from F to Li.

TABLE I. Shown are the angles θ_{max} and θ_{min} (in deg) which refer to the maxima and minima of the interference structures observed in the angular distributions of the Auger electrons of the LiF $^1\Sigma(3\sigma^{-2})$ state and the corresponding HF $^1\Sigma(2\sigma^{-2})$ state. The symbols k or k_{av} indicate that the positions of the extrema are evaluated according to Eqs. (3.1) and (3.2) by employing the asymptotic wave number or the averaged wave number (see text). The positions of the extrema that are deduced from a full numerical calculation (after subtraction of the background) are shown in the rows labeled with f.

Extremum \ n	0	1	2	3	4	5	6
LiF: θ_{max},k	0.00	47.15	68.89	87.69	106.24	126.84	156.86
LiF: θ_{max},k_{av}	0.00	45.05	65.60	83.13	100.02	117.86	139.54
LiF: θ_{max},f	0.00	42.25	63.75	82.00	99.60	118.25	141.15
LiF: θ_{min},k	32.85	58.66	78.45	96.87	116.08	139.42	
LiF: θ_{min},k_{av}	31.43	55.96	74.55	91.56	108.70	127.89	155.18
LiF: θ_{min},f	28.10	53.70	73.05	90.75	108.60	128.65	157.00
HF: θ_{max},k	0.00	63.23	95.70	130.47			
HF: θ_{max},k_{av}	0.00	58.77	87.88	116.39	157.83		
HF: θ_{max},f	0.00	57.65	89.70	122.05	a		
HF: θ_{min},k	43.51	79.89	111.97	157.50			
HF: θ_{min},k_{av}	40.60	73.87	101.76	133.26			
HF: θ_{min},f	39.05	73.15	102.50	137.10			

[a] Not found since the curve is too flat (see Fig. 2).

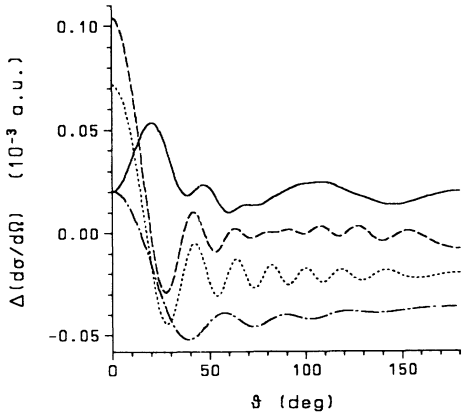

FIG. 2. For several dicationic final states we show the difference of the angular distribution of the full calculation and the nonconstant background. Shown are the results of the following states of the LiF molecule: $^1\Pi(4\sigma^{-1},1\pi^{-1})$ (solid line), $^1\Sigma(3\sigma^{-1},4\sigma^{-1})$ (dashed line), and $^1\Sigma(3\sigma^{-2})$ (dotted line). The result of the $^1\Sigma(2\sigma^{-2})$ state of the HF molecule is illustrated by the dashed-dotted curve. In order to make the comparison easier we have shifted the curves vertically with respect to each other. Without these shifts all curves oscillate around zero. Due to the shorter internuclear distance of the HF molecule, one observes an interference structure with a longer wavelength (compare the dotted with the dashed-dotted curve). Note that the amplitudes of the oscillations of the HF distribution are smaller in comparison to the LiF distributions. This is because the H atom is a weaker scatterer than the Li atom. It is interesting to note that one is able to detect an interference structure even in the Π states (see solid line). Without background subtraction this interference structure would be invisible (compare with Fig. 3). The phase jump that appears in the dashed curve is discussed in the text.

(2.7)–(2.11) one readily arrives at the conclusion that the basic structure of the angular distribution should be proportional to $|Y_{1,0}(\Omega)|^2$. By the same argument one expects the basic structure of the $^1\Sigma(4\sigma^{-2})$ and $^1\Sigma(1\pi^{-1},1\pi^{-1})$ states to be proportional to $|Y_{2,0}(\Omega)|^2$ and $^1\Pi(3\sigma^{-1},1\pi^{-1})\sim|Y_{1,1}(\Omega)|^2$, $^1\Pi(4\sigma^{-1},1\pi^{-1})\sim|Y_{2,1}(\Omega)|^2$, and $^1\Delta(1\pi^{-2})\sim|Y_{2,2}(\Omega)|^2$. There is no difference in the basic structure between singlet and triplet states. We have found that the function $|Y_{1,0}(\Omega)|^2$ when properly normalized is almost indistinguishable from the plane-wave result shown in Fig. 1(b) (dotted line). Because of the nodal plane present in the 4σ orbital (we recall again that the 4σ orbital is similar to the fluorine p_z orbital) one observes a phase jump in the oscillation structure. Comparing the difference function (see Fig. 2) of the $^1\Sigma(3\sigma^{-1},4\sigma^{-1})$ state with the one of the $^1\Sigma(3\sigma^{-2})$ state one finds that the oscillations are in phase for angles below 90° and of opposite phase for angles above 90°. In general, the inspection of Fig. 1(b) leads to similar conclusions as before. The neglect of the electron-molecule scattering potential leads essentially to a basic structure and the inclusion of this potential enhances the intensity in the forward direction (i.e., toward the Li atom) and introduces interference structures. Similar observations can be made for the other angular distributions as well. However, the influence of the interaction potential becomes weaker for final Π and Δ states.

When computing the differential Auger rates one should, in principle, use the static-exchange potential of the particular final state under discussion. Fortunately, we have found that the dependence of the differential rates on the fine details of the potential is rather weak and one may use the same potential for the computation of several distributions. We have used the potential of

the $^1\Sigma(3\sigma^{-2})$ state for computing the rates of all states that are discussed in this section. Only for Li core-hole states, which are discussed in the next section, we used the potential of the $^1\Sigma(2\sigma^{-2})$ state as well. Figure 3 shows the differential Auger rates of LiF for all final states except those with a 2σ hole. The distributions are compared with those of the HF molecule. Since the Auger process is mainly an atomic process, the distributions are quite similar for both molecules. However, the hydrogen atom is a weaker scatterer than the Li atom and hence one observes a weaker interference structure in the HF rates. The difference in the period of the oscillations shows once more that the interference structure is a finger print of the nuclear geometry (see also Fig. 2). Thus one can determine the nuclear geometry from the interference structure. The shape of the distribution of a triplet state is quite similar to the one of the corresponding singlet state. The large difference in magnitude between the LiF $^3\Pi(4\sigma^{-1},1\pi^{-1})$ and the HF $^3\Pi(3\sigma^{-1},1\pi^{-1})$ states may require some explanation. These two states correlate with the $^3D(p^{-1},p^{-1})$ state of F^- which is dark due to symmetry considerations. Now LiF has a much longer bond length than HF and the LiF bond is more ionic than the HF bond. This makes the LiF 4σ orbital resemble the p_z orbital of F^- more closely than does the HF 3σ orbital. Consequently, the LiF $^3\Pi(4\sigma^{-1},1\pi^{-1})$ state has a smaller Auger rate than the HF $^3\Pi(3\sigma^{-1},1\pi^{-1})$ state.

V. FINAL DICATIONIC STATES WITH A Li CORE HOLE

Final dicationic states which are characterized by a 2σ hole are produced with a very low Auger rate. The 2σ

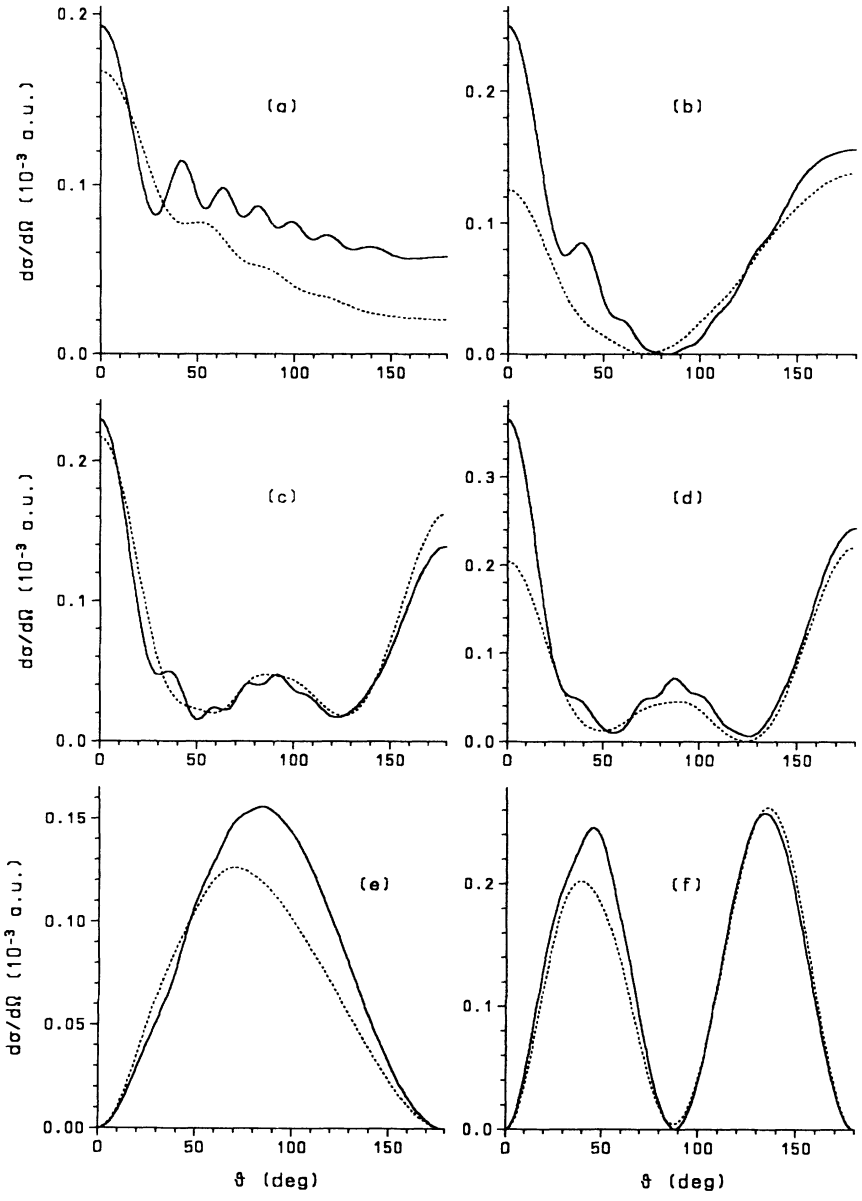

FIG. 3. Shown are the computed angularly resolved Auger spectra of the LiF molecule (solid line) and the HF molecule (dotted line). The angular distributions of the following LiF states { HF states }: (a) $^1\Sigma(3\sigma^{-2})$ $\{^1\Sigma(2\sigma^{-2})\}$, (b) $^1\Sigma(3\sigma^{-1},4\sigma^{-1})$ $\{^1\Sigma(2\sigma^{-1},3\sigma^{-1})\}$, (c) $^1\Sigma(1\pi^{-1},1\pi^{-1})$ $\{^1\Sigma(1\pi^{-1},1\pi^{-1})\}$, (d) $^1\Sigma(4\sigma^{-2})\{^1\Sigma(3\sigma^{-2})\}$, (e) $^1\Pi(3\sigma^{-1},1\pi^{-1})$ $\{^1\Pi(2\sigma^{-1},1\pi^{-1})\}$, (f) $^1\Pi(4\sigma^{-1},1\pi^{-1})$ $\{^1\Pi(3\sigma^{-1},1\pi^{-1})\}$, (g) $^3\Sigma(3\sigma^{-1},4\sigma^{-1})$ $\{^3\Sigma(2\sigma^{-1},3\sigma^{-1})\}$, (h) $^3\Pi(3\sigma^{-1},1\pi^{-1})$ $\{^3\Pi(2\sigma^{-1},1\pi^{-1})\}$, (i) $^3\Pi(4\sigma^{-1},1\pi^{-1})$ $\{^3\Pi(3\sigma^{-1},1\pi^{-1})\}$, and (j) $^1\Delta(1\pi^{-2})$ $\{^1\Delta(1\pi^{-2})\}$ are depicted.

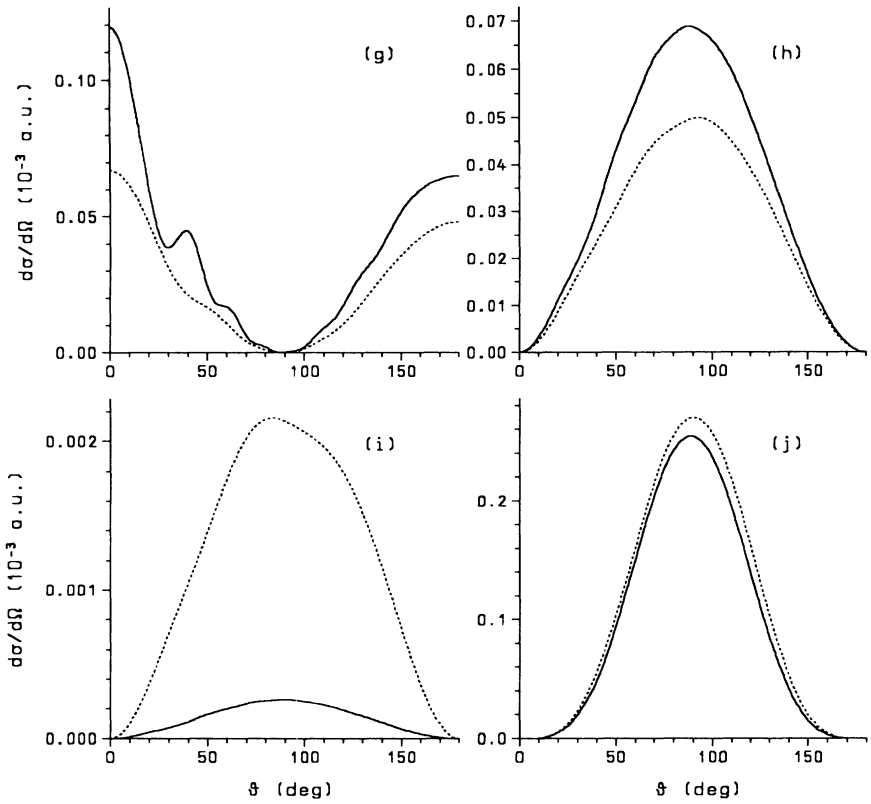

FIG. 3. (*Continued*).

orbital is the Li-core orbital and it is the only molecular orbital which is located at the Li nucleus. The final $^1\Sigma(2\sigma^{-2})$ state is produced by an extremely low rate ($\leq 3\times 10^{-9}$ a.u.) and we could not determine this rate unambiguously. The rates leading to final states with only one 2σ hole are much larger than the just mentioned rate but they are still very low and may thus not be accessible experimentally. However, the angularly resolved rates of these states show quite interesting structures that we would like to discuss.

Figure 4 depicts the angularly resolved rates belonging to final states containing a single 2σ hole. To be specific let us discuss the angular distribution belonging to the $^1\Pi(2\sigma^{-1},1\pi^{-1})$ final state. As described in Sec. II there are two Coulomb matrix elements contributing to this rate [see Eq. (2.7)], namely the integral $V(\varepsilon,l,m)_{2\sigma,1\pi}$ and $V(\varepsilon,l,m)_{1\pi,2\sigma}$. The first integral represents the process where the 2σ electron fills the 1σ hole and the π electron is ejected, i.e., the Auger electron originates from the vicinity of the F nucleus. The second integral represents the process where the π electron fills the 1σ hole and the 2σ electron is ejected, i.e., here the Auger electron originates from the vicinity of the Li nucleus. The interference of these two different paths creates the oscillations. Note that, in contrast to the spectra discussed in Sec. III, the oscillations are not created by the scattering potential; they remain when the plane-wave approximation is used. The scattering potential, however, does change the interference structure quite strongly and an interpretation of the angular distribution becomes rather involved. We consider it not useful to discuss all these details but emphasize again that for the spectra under discussion there is a different physical mechanism for creating the interference structure.

We have already mentioned that, in general, it is unnecessary to use the static-exchange potential generated by the charge distribution of the particular final state under discussion in order to compute reliable differential Auger rates. In the previous chapter we thus have used the $^1\Sigma(3\sigma^{-2})$ potential for computing all rates. Turning to final states containing a 2σ hole the situation changes somewhat. Removing an electron from a Li-centered orbital changes the potential in a different way than removing an electron from a F-centered orbital, e.g., the dipole moments of the resulting scattering potentials are quite different. Since experiments are unavailable, we do not consider it worthwhile to evaluate all these differential rates with respect to their correct potential. We rather evaluated the rates with respect to the $^1\Sigma(3\sigma^{-2})$ potential (solid lines) and the $^1\Sigma(2\sigma^{-2})$ potential (dashed lines). Both potentials are of course "incorrect" but the use of the correct potentials will yield distributions which lie between these two *limiting* cases. By comparing the solid and dashed curves in Fig. 4 one observes that the use of the $^1\Sigma(2\sigma^{-2})$ potential increases the intensity in the forward direction more strongly. This is easy to explain. The $^1\Sigma(2\sigma^{-2})$ potential is more attractive in the vicinity of the Li nucleus compared to the $^1\Sigma(3\sigma^{-2})$ potential. This deflects the Auger electrons into the forward direction.

V. THE ANGULARLY INTEGRATED AUGER SPECTRUM OF LiF

The emphasis of the present paper is on the investigation of the angular distribution of Auger electrons. For the sake of completeness, however, we would like to discuss the angularly integrated Auger spectrum of LiF as well (for HF see Ref. [10]). We start with some technical remarks, discuss the Auger energies, and then turn to the integrated Auger intensities. We like to mention that the integrated Auger rates of LiF have recently been investigated by Colle and Simonucci [14].

An uncontracted Gaussian basis set is used in all our LiF calculations. It consists of $13s/8p$ Cartesian Gaussian functions [15] centered at the F nucleus and of $13s$ [15] and $5p$ [16] Gaussians centered at the Li nucleus. The internuclear distance was set to $R=2.955$ a.u. With the above basis set we have performed separate self-consistent-field calculations for each initial and final state employing two different Hartree-Fock procedures. The energy of the ionic *initial* state $^2\Sigma(1\sigma^{-1})$ and for completeness also of $^2\Sigma(2\sigma^{-1})$ are computed with the conventional restricted Hartree-Fock (RHF) procedure while the energies of the *final* dicationic states are computed with the spin-averaged Hartree-Fock (SAHF) method which is described in Ref. [10]. These energies are shown in the second column of Table II. The advantage of the SAHF procedure is that it converges faster and that there are fewer calculations than in the RHF procedure because there is only one orbital set for both the singlet and the corresponding triplet states. But both the restricted and the spin-averaged SCF methods yield virtually the same energies (see Ref. [10]). The Auger energies of the third column are the difference of the energy of the ionic initial state $^2\Sigma(1\sigma^{-1})$ and the dicationic final state under discussion.

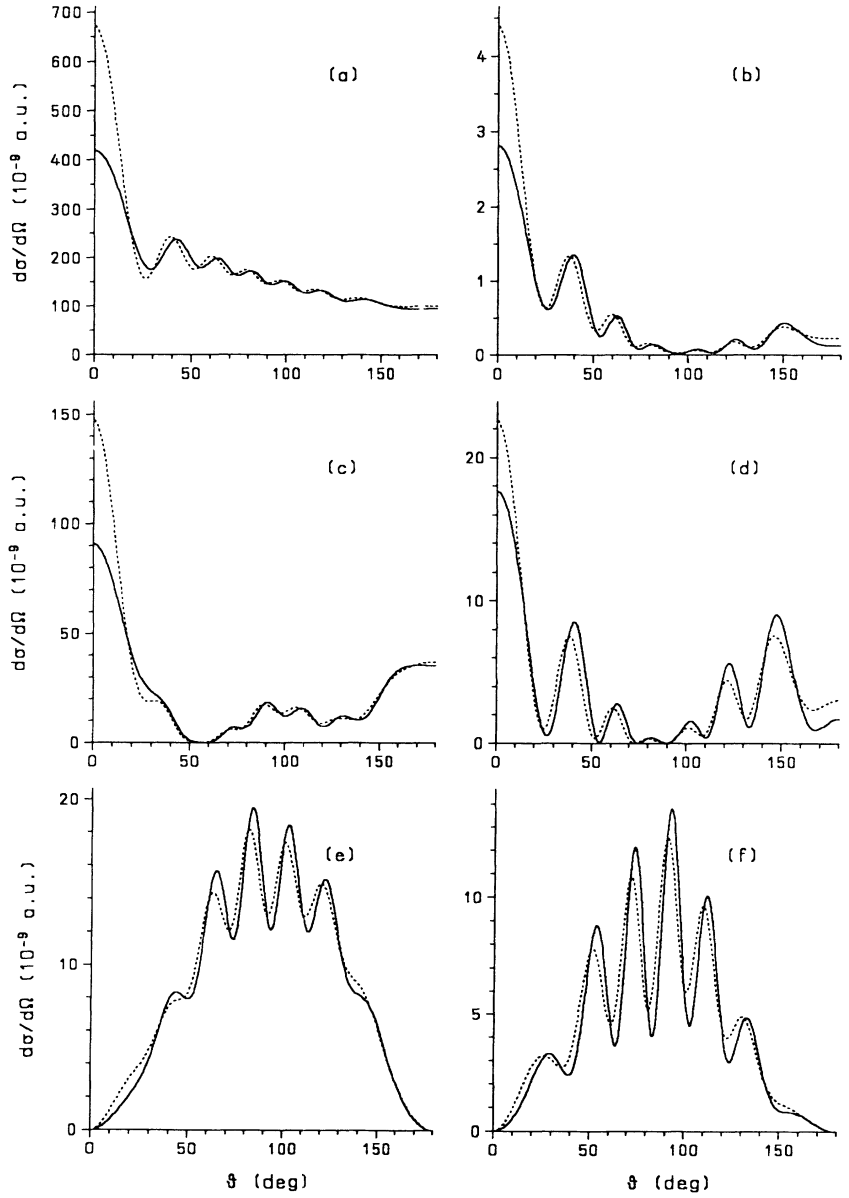

FIG. 4. Shown are the computed angularly resolved Auger spectra of those LiF states that contain a 2σ hole. Compared are the results of two calculations using different potentials for the electron-molecule interaction, i.e., the $^1\Sigma(3\sigma^{-2})$ potential (solid line) or the $^1\Sigma(2\sigma^{-2})$ potential (dotted line). Shown are the angular distributions of the following states: (a) $^1\Sigma(2\sigma^{-1},3\sigma^{-1})$, (b) $^3\Sigma(2\sigma^{-1},3\sigma^{-1})$, (c) $^1\Sigma(2\sigma^{-1},4\sigma^{-1})$, (d) $^3\Sigma(2\sigma^{-1},4\sigma^{-1})$, (e) $^1\Pi(2\sigma^{-1},1\pi^{-1})$, and (f) $^3\Pi(2\sigma^{-1},1\pi^{-1})$. Note that the left-hand side refers to singlet while the right-hand side refers to triplet states.

TABLE II. Shown are total energies (in a.u.), Auger transition energies (in eV), and angularly integrated Auger rates (in 10^{-3} a.u.). The second column shows the SCF energies of the states that are defined in the first column. The energies of the core-ionized states are computed with the RHF procedure and the energies of the dicationic state are evaluated by SAHF (see text). The third column shows the ΔSCF Auger energies (in eV), i.e., the difference between the energies of the dicationic states and the energy of the initial $^2\Sigma(1\sigma^{-1})$ state. The fourth column shows the ADC double-ionization energies to which 686.66 eV has been added. The fifth column shows the experimentally determined Auger energies of Hotokka *et al.* [18] and the two last columns give the computed angularly integrated Auger rates (in 10^{-3} a.u.). The numbers in brackets indicate a multiplicative power of ten.

State	$\text{Total}_{\text{SCF}}$ energies (a.u.)	Auger energies (eV)			Rates (10^{-3} a.u.)	
		ΔSCF	ADC(2)	Expt.	RHF	SAHF
$^3\Sigma^-(1\pi^{-1},1\pi^{-1})$	−105.7149	652.28	651.13	652.18	0.000	0.000
$^3\Pi(4\sigma^{-1},1\pi^{-1})$	−105.7040	651.98	650.69	650.34	0.002	0.002
$^1\Delta(1\pi^{-2})$	−105.6182	649.65	648.47	648.47	1.712	1.751
$^1\Pi(4\sigma^{-1},1\pi^{-1})$	−105.6046	649.28	647.99	647.66	1.697	1.734
$^1\Sigma^+(4\sigma^{-2})$	−105.5437	647.62	647.92	646.64	0.676	0.689
$^1\Sigma^+(1\pi^{-1},1\pi^{-1})$	−105.5215	647.02	645.30	644.82	0.521	0.530
$^3\Pi(3\sigma^{-1},1\pi^{-1})$	−104.9130	630.46	630.06	630.46	0.579	0.443
$^3\Sigma^+(3\sigma^{-1},4\sigma^{-1})$	−104.8900	629.83	629.63	629.62	0.286	0.219
$^1\Pi(3\sigma^{-1},1\pi^{-1})$	−104.5425	620.38	620.74	621.85	1.305	1.059
$^1\Sigma^+(3\sigma^{-1},4\sigma^{-1})$	−104.5293	620.02	620.28	620.26	0.652	0.529
$^3\Pi(2\sigma^{-1},1\pi^{-1})$	−103.9145	603.29			0.072[−3]	0.054[−3]
$^1\Pi(2\sigma^{-1},1\pi^{-1})$	−103.9134	603.26			0.141[−3]	0.113[−3]
$^3\Sigma^+(2\sigma^{-1},4\sigma^{-1})$	−103.8652	601.95			0.034[−3]	0.025[−3]
$^1\Sigma^+(2\sigma^{-1},4\sigma^{-1})$	−103.8358	601.15			0.173[−3]	0.166[−3]
$^1\Sigma^+(3\sigma^{-2})$	−103.8090	600.42	600.94	602.62	1.020	0.788
$^3\Sigma^+(2\sigma^{-1},3\sigma^{-1})$	−103.0031	578.49			0.004[−3]	0.003[−3]
$^1\Sigma^+(2\sigma^{-1},3\sigma^{-1})$	−102.9839	577.96			2.014[−3]	1.549[−3]
$^1\Sigma^+(2\sigma^{-2})$	−100.6523	514.52				
$^2\Sigma^+(2\sigma^{-1})$	−104.6302					
$^2\Sigma^+(1\sigma^{-1})$	−81.7445					

A more advanced way to calculate the Auger energies is to employ a Green's-function method. The algebraic diagrammatic construction (ADC) [5] is particularly useful for that purpose. The ADC method, however, yield double-ionization energies rather than Auger energies. In order to account for the energy acquired by core ionization we have therefore shifted the double-ionization energies of Ref. [17] to coincide with the measured Auger energy of the $^1\Delta(1\pi^{-2})$ state. The resulting ADC Auger energies are displayed in column 4 of Table II. The experimental values of the Auger energies are taken from Ref. [18] and are reproduced in column 5. The comparison of the different Auger energies shows that the agreement between the theoretical and experimental ones is quite good. Not that the computed energies of the $^1\Sigma(4\sigma^{-2})$ and $^1\Sigma(1\pi^{-1},1\pi^{-1})$ are rather close together on the change in self-consistent-field (Δ SCF) level and well separated on the ADC level. From a theoretical point of view it is expected that the energies of the second-order ADC scheme [ADC(2)] are better than the ΔSCF ones. This is also found by considering the span of the computed Auger energies [from $^1\Sigma(3\sigma^{-2})$ to $^1\Delta(1\pi^{-2})$] which is too large by 3.38 eV for the ΔSCF energies but only too large by 1.68 eV for the ADC(2) energies. Moreover, there are three ADC(2) energies close to 648 eV. This increases the convoluted rate in the vicinity of 648 eV yielding an improved theoretical spectrum.

We would like to emphasize that the individual Auger lines are rarely resolved experimentally. The energy position, intensity, and width of each line (i.e., transition) is evaluated by a fitting procedure after the subtraction of a non-well-defined background. The experimentally deduced energies and, in particular, intensities of close-lying lines and/or lines of low intensity may thus be subject to considerable errors and should be handled with care. On the other hand, care must also be taken when comparing the experimental energies with computed fixed-nuclei data. The individual computed lines are subject to shifts owing to the nuclear dynamics [6].

We have found [10] that the computed rates are very insensitive to the choice of the specific Hartree-Fock procedure applied to the *final* states. Thus we have used the SAHF orbitals of the final state under discussion for the calculation of all Auger rates (Table II). For the *initial* (core-ionized) state, however, we used the RHF and the SAHF orbitals. The resulting integrated rates are shown in the last two columns of Table II. As for the HF molecule [10] we find a noticeable effect only on the rates of those final states that contain an inner valence hole (2σ or 3σ). These rates are decreased when using the SAHF orbitals for the *initial* state yielding results which compare better with experiment. A similar observation was made for the HF molecule [10]. The differences between the RHF and SAHF rates reflect the limitations of the one particle picture for the *initial* state. Only the use of a correlated initial state in the calculation of the rates will remove this ambiguity.

We finally compare the experimental spectrum [18] with the theoretical one. Because our emphasis is on the Auger rates we felt free to use the ADC(2) energies rather

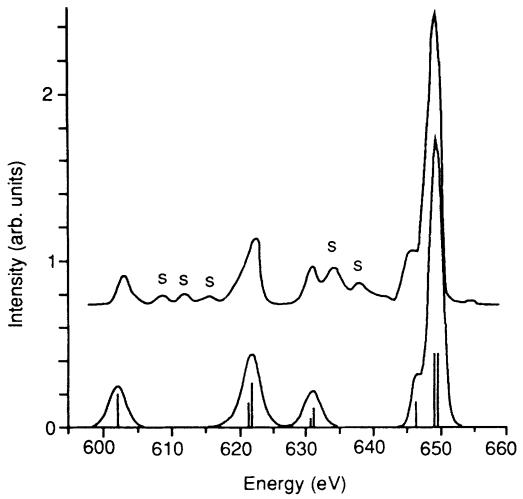

FIG. 5. Comparison of the computed Auger spectrum of LiF with experimental data. In order to be more easily comparable to the experimental data we have convoluted the computed stick spectrum with normalized Gaussian functions of full widths at half maxima: 3.0 eV for the states $^1\Sigma(3\sigma^{-2})$, $^1\Sigma(2\sigma^{-1},4\sigma^{-1})$, $^3\Sigma(2\sigma^{-1},4\sigma^{-1})$, $^1\Pi(2\sigma^{-1},1\pi^{-1})$, and $^3\Pi(2\sigma^{-1},1\pi^{-1})$, 5.0 eV for the $^1\Sigma(3\sigma^{-1},4\sigma^{-1})$ state, 2.9 eV for the states $^3\Sigma(3\sigma^{-1},4\sigma^{-1})$, $^1\Pi(3\sigma^{-1},1\pi^{-1})$, and $^3\Pi(3\sigma^{-1},1\pi^{-1})$, 1.7 eV for the $^1\Sigma(1\pi^{-1},1\pi^{-1})$ state, and 2.2 eV for the states $^1\Sigma(4\sigma^{-2})$, $^1\Pi(4\sigma^{-1},1\pi^{-1})$, $^3\Pi(4\sigma^{-1},1\pi^{-1})$, and $^1\Delta(1\pi^{-2})$. The rates employed for the theoretical curve are those obtained by using the SAHF orbitals (see Table II) while the energies used are the ADC(2) results of Table II. The envelope of both the theoretical and experimental spectra is given in arbitrary units. The peaks in the experimental spectrum marked with *s* originate from shake-off and shake-up satellites.

than the ΔSCF ones when comparing to experiment. The SAHF rates are convoluted with Gaussian functions in order to make this comparison more vivid. Figure 5 shows that the agreement with experiment is good. The missing lines can be attributed to shake-off and shake-up satellites [14,18] and do not arise from the decay of the core-ionized state discussed here. A similar situation was met when studying the Auger spectrum of the HF molecule [10]. It should be noted that, in principle, these satellite lines can be eliminated from the spectrum experimentally if the Auger electron is measured in coincidence with the primary electron ejected from the core orbital. Of course, these satellite lines can also be calculated [14].

VI. CONCLUDING REMARKS

In principle, Auger angular distributions can be measured by coincidence techniques or by adsorbing the molecule in a well-defined configuration. We have computed and analyzed the angular distributions of Auger electrons of LiF and HF. Since these molecules are ionic and their molecular orbitals have a strong atomic character simple angular-momentum considerations have been helpful in the interpretation of the results. The fact that the Auger electron feels the molecular scattering potential modifies considerably the angular distributions. The most interesting modification is the appearance of oscillations in the angular distributions. These oscillations are caused by the interference of the direct path of the Auger electron with the path that is deflected by the Li nucleus. Consequently, the interference patterns dependent on the internuclear distance, and, in favorable cases, the internuclear distance can be determined from the interference pattern. The situation is somewhat related to the findings in extended x-ray absorption fine-structure (EXAFS) spectra where multiple scattering is of relevance [19]. Another modification is the enhancement of intensity in the forward direction (from F to Li). In general, we have found that the influence of the scattering potential is stronger the higher is the electronic energy of the final dicationic ion. Another rule of thumb is that the influence of this potential is more important for Σ states than for Π or Δ states.

A particularly interesting and new type of interference structures appears when the two holes of the final state of the Auger decay are located at different nuclei, i.e., of the F and Li nuclei in the present calculations. In this case the Auger electron may originate either from the vicinity of the F or from the Li nucleus and the resulting two pathways interfere. Note that this interference pattern, which can be quite strong, is not created by the electron-molecule interaction potential, although it is, of course, modified by this potential.

The latter type of oscillation is expected to be most pronounced for diatomic homonuclear molecules. In this case the molecular orbitals have an equal weight on both centers and the Auger electrons will originate with equal weight from both centers. This may lead to strong interference structures with vanishing intensity at certain angles. These expectations give rise to the prediction of a third type of oscillations which we expect to find in the angular distribution of the autoionizing electron when considering the decay of a state of proper gerade or ungerade symmetry. For this purpose the homonuclear molecule should be initially core excited (by photons, for instance) to ensure a well-defined symmetry of the decaying state.

The modification of the scattered wave by the scattering potential holds, of course, independently of the ionization process. The interference structure should hence be observable for, e.g., photoionization processes as well.

ACKNOWLEDGMENT

We thank the Deutsche Forschungsgemeinschaft (DFG) for financial support.

[1] R. Spohr, T. Bergmark, N. Magnusson, L. Werme, C. Nordling, and K. Siegbahn, Phys. Scr. **2**, 31 (1970); W. Moddeman, T. Carlson, M. Krause, B. Pullen, W. Bull, and G. Schweitzer, J. Chem. Phys. **55**, 2317 (1971); R. W. Shaw and T. D. Thomas, Phys. Rev. A **11**, 1491 (1975); H. Siegbahn, L. Asplund, and P. Kelfve, Chem. Phys. Lett. **35**, 330 (1975); J. White, R. Rye, and J. Houston, *ibid.* **46**, 146 (1977); R. Rye, T. Madey, J. Houston, and P. Hollo-

way, J. Chem. Phys. **69**, 1504 (1978); P. Kelfve, B. Blomster, H. Siegbahn, K. Siegbahn, E. Sanhueza, and O. Goscinski, Phys. Scr. **21**, 75 (1980); V. Carravetta and H. Ågren, Phys. Rev. A **35**, 1022 (1987).

[2] T. Aberg and G. Howat, *Theory of the Auger Effect,* edited by S. Flügge, Handbuch der Physik Vol. 31 (Springer, Berlin, 1982), and references therein.

[3] G. Howat, T. Aberg, and O. Goscinski, J. Phys. B **11**, 1575 (1978); K. Faegri, Jr. and H. P. Kelly, Phys. Rev. A **19**, 1649 (1979); D. R. Jennison, Chem. Phys. Lett. **69**, 435 (1980); M. Higashi, E. Hiroike, and T. Nakajima, Chem. Phys. **68**, 377 (1982); R. Manne and H. Ågren, Chem. Phys. Lett. **93**, 201 (1985); F. P. Larkins and J. A. Richards, Aust. J. Phys. **39**, 809 (1986); V. Carravetta and H. Ågren, Phys. Rev. A **35**, 1022 (1987); R. Colle and S. Simonucci, *ibid.* **39**, 6247 (1989).

[4] I. Hillier and J. Kendrick, Mol. Phys. **31**, 849 (1975); K. Faegri, Jr., Chem. Phys. Lett. **46**, 541 (1977); N. Kosugi, T. Ohta, and H. Kuroda, Chem. Phys. **50**, 373 (1980); H. Ågren, J. Chem. Phys. **75**, 1267 (1981), and references therein.

[5] F. Tarantelli, A. Tarantelli, A. Sgamellotti, J. Schirmer, and L. Cederbaum, J. Chem. Phys. **83**, 4683 (1985).

[6] L. S. Cederbaum, P. Campos, F. Tarantelli, and A. Sgamellotti, J. Chem. Phys. **95**, 6634 (1991).

[7] M. Ya. Amusia, Comments At. Mol. Phys. **8**, 61 (1979); D. Lindle, T. Ferrett, U. Becker, P. Kobrin, C. Truesdale, H. Kerkhoff, and D. Shirley, Phys. Rev. A **31**, 714 (1985), and references therein; U. Becker (private communication).

[8] Zhou Ru-Hong and Cao Pei-Lin, Surf. Sci. **243**, L49 (1991).

[9] S. Mórz, A. Mórz, A. Wieczorek, and V. Fritzsche, Surf. Sci. **224**, 243 (1989), and references therein; R. Rydgren, H. Helbig, and C. Moyer, Surf. Sci. **244**, 81 (1991).

[10] K. Zähringer, H.-D. Meyer and L. S. Cederbaum, Phys. Rev. A **45**, 318 (1992).

[11] N. F. Lane, Rev. Mod. Phys. **52**, 29 (1981).

[12] S. Hara, J. Phys. Soc. Jpn. **22**, 710 (1967).

[13] H.-D. Meyer, Phys. Rev. A **34**, 1797 (1986).

[14] R. Colle and S. Simonucci, Phys. Rev. A **42**, 3913 (1990).

[15] F. B. van Duijneveldt (unpublished).

[16] R. Colle, S. Simonucci, and T. Woodruff, Phys. Rev. A **38**, 694 (1988).

[17] F. Tarantelli (private communication).

[18] M. Hotokka, H. Ågren, H. Aksela, and S. Aksela, Phys. Rev. A **30**, 1855 (1984).

[19] B. K. Theo, *EXAFS: Basic Principles and Data Analysis* (Springer, Berlin, 1986).